PERGAMON

International Journal of Solids and Structures 37 (2000) 6085–6105

INTERNATIONAL JOURNAL OF SOLIDS and STRUCTURES

www.elsevier.com/locate/ijsolstr

A Monte Carlo solution method for linear elasticity

D. Shia, C.Y. Hui*

Department of Theoretical and Applied Mechanics, 212 Kimball Hall, Cornell University, Ithaca, NY 14853, USA

Received 23 March 1999; in revised form 24 June 1999

Abstract

A probabilistic method is proposed and implemented to solve linear elasticity problems. The method, called walk on the boundary method (WBM), uses the same governing equations as the boundary element method. Unlike in finite element and boundary element methods, WBM does not require any meshing. Also, error estimates for WBM are easier to obtain than in finite element and boundary element methods. Furthermore, WBM obtains a point solution at a specific point of interest instead of a full field solution as in finite element and boundary element methods. WBM is developed for general traction boundary value problems in antiplane shear, plane strain, and 3D elasticity. Numerical implementations are performed for three example problems: (1) antiplane shear problem with a centrally located circular hole being loaded by uniformly applied traction, (2) plane strain problem with centrally located circular hole being loaded by uniform tension, and (3) 3D elasticity problem with a centrally located spherical cavity being loaded by uniform tension. Results from the three example problems compared favorably with results from the analytical and finite element solution. Three critical issues associated with the WBM for linear elasticity are pointed out for its further improvement.

Keywords: Monte Carlo method; Elasticity; Random walk

1. Introduction

The two most popular schemes to solve elasticity problems in solids are the finite element method and the boundary element method. The finite element method (FEM) has the advantage that it is very versatile but requires meshing the whole domain of interest. This limits the degree of geometrical complexities that it can practically simulate. The boundary element method (BEM) is better than the finite element method (FEM) for elasticity problems in the sense that it only needs the boundaries of the

* Corresponding author. Fax: +1-607-255-2011.
E-mail address: ch45@cornell.edu (C.Y. Hui).

0020-7683/00/$ - see front matter
PII: S0020-7683(99)00263-2

domain of interest to be meshed. This allows BEM to be more versatile than FEM in modeling problems with geometrical complexities.

Often in engineering applications, we are only interested in the state of deformation at specific points in the body. However, in order to obtain this solution via FEM, a full field analysis must be carried out even though only a very small portion of the solution is actually needed. In BEM the solution of displacement and traction fields on the boundary of the domain is required before stress at the point of interest can be computed. Thus, in both FEM and BEM, greater part of the computation is usually involves in solving for displacement and stress fields away from the point of interest. In this paper, we will present a numerical scheme that requires neither meshing nor computing all of the field quantities.

The numerical method presented here is based on simulating a random walk on the boundary of the domain of interest, hence the name 'walk on the boundary method' (WBM). The method is used mostly by physicists and nuclear engineers to solve heat transfer and neutron transport problems (Sabelfeld, 1991; Nakamura, 1977; Hoffman and Banks, 1976; Zagajac, 1996). In order to apply the WBM, the physical problem is formulated using the integral equation approach. For elasticity problems, the formulation completely resembles that of the BEM. Numerically, there is one major difference; unlike BEM, WBM does not require the discretization of the boundary in order to obtain solutions. Moreover, the field quantity of interest (displacement or stress) in WBM can be obtained at exactly the point of interest by sampling displacement and/or traction values on the boundary through simulated random walks on the boundary. Because WBM does not require meshing and can obtain solutions at a specific point, it can be a very efficient numerical scheme when complex geometries, e.g., oddly shaped bodies containing many holes, are involved. Another advantage of the WBM is that error estimates are much easier to obtain than in FEM and BEM.

WBM is a probabilistic method for solving deterministic problems based on global integral equations. The integral equations are called global because they are applied to the entire domain of interest. Another probabilistic method for solving deterministic problems based on integral equations is called the 'walk inside the domain algorithm' (Sabelfeld, 1991) or the 'floating random walk' (Haji-Sheikh and Sparrow, 1966; Brown, 1956). The method is based on the local integral mean-value relationship. The floating random walk allows large random steps for points far removed from the boundary; however, as the walker approaches the boundary, smaller steps are needed. Also, for complex geometries, considerable computer time is required to determine the closest boundary point from the current walker position in order to construct the circle (Hoffman and Banks, 1976). There are also other probabilistic methods for solving deterministic problems which are based on partial differential equations. A well known probabilistic method is the solution of the Laplace equation with Dirichlet boundary conditions by simulating a discrete random walk (Farlow, 1993; Minkowycz et al., 1988). More recently, Grigoriu has presented a probabilistic method based on Ito's formula (Grigoriu, 1997). This probabilistic method obtains point solutions to second order parabolic and elliptic partial differential equations with Dirichlet or Neumann boundary conditions by simulating Brownian motion. A major drawback of both of these methods is that their applicability is limited, so far, only to uncoupled, second order parabolic and elliptic differential equations. Therefore, these methods can solve only a limited class of problems in elasticity, such as torsion or antiplane shear problems. If we insist on a formulation of elasticity based on partial differential equations, we will need a probabilistic method for solving fourth order elliptic partial differential equations in plane problems (biharmonic equations), or three coupled second order elliptic equations in 3D (Navier equations). This problem is still unsolved since both the biharmonic and Navier equations do not lend themselves easily to a probabilistic interpretation. The integral equation formulation does not have this problem (Sabelfeld, 1991). Integral equations lend themselves easily to probabilistic interpretation, even for 3D elasticity problems.

In the following sections of the paper, a theoretical background of the WBM is presented. Following the theory section, we will show how the WBM can be applied to solve elasticity problems formulated

using global integral equations. Three numerical examples are presented: (1) Antiplane shear problem of a square containing a centrally located circular hole; (2) Plane strain problem of a square containing a centrally located circular hole; (3) 3D elasticity problem of a cube containing a centrally located spherical cavity. These problems are chosen because the numerical results can be compared to the available analytical results for each of the problems, except for the 3D problem where finite element results are used. In the last section, we will show how error estimates can be obtained.

2. Theoretical background of WBM

The theory of the WBM is summarized in this section. For more details, the reader is referred to Sabelfeld (1991) and Nakamura (1977). First, we will present the type of equations that the WBM is designed to solve. Then, we will describe the probabilistic basis of the WBM and discuss its implementation.

2.1. Fredholm integral equations of the second kind

The equations that the WBM is designed to solve are Fredholm integral equations of the second kind. The properties of Fredholm integral equations are well known and can be found in many applied mathematics text books (Hilderbrand, 1965; Kanwal, 1997). In this section, we will focus on the aspects most relevant to the WBM.

It is well known that the equations of linear elasticity can be written in the following form over a domain Ω with boundary Γ

$$\mu(\bar{x}') = \int_{\Gamma} K(\bar{x}', \bar{y})\mu(\bar{y})\, \mathrm{d}s_{\bar{y}} + f(\bar{x}'), \quad \bar{x}' \in \Gamma \tag{1}$$

where μ is the unknown density function on the boundary, $\bar{x}'$is a point on the boundary,$\bar{y}$ is the dummy integration variable, K is the kernel, e.g., the Kelvin solution in elasticity and f is a known function on the boundary. Note that Eq. (1) is a Fredholm integral equation of the second kind (Hilderbrand, 1965; Kanwal, 1997). Both μ and f may be scalar-valued or vector-valued functions; when μ and f are scalar-valued functions,$K(\bar{x}, \bar{y})$ is also a scalar-valued function; when μ and f are vector-valued functions with dimension n, the kernel is a $n \times n$ matrix and the integration is performed over each element of the matrix. Specific examples of K and μ for linear elasticity are given in Section 3 for antiplane shear, plane strain and 3D elasticity.

In order to simplify subsequent presentation of the paper, we will adopt the following operator notation

$$\mathbf{K}\mu \equiv \int_{\Gamma} K(\bar{x}, \bar{y})\mu(\bar{y})\, \mathrm{d}s_{\bar{y}} \tag{2}$$

where the bold letter $\mathbf{K}$ denotes the integral operator. Eq. (1) can now be rewritten as

$$(\mathbf{I} - \mathbf{K})\mu = f \tag{3}$$

where $\mathbf{I}$ is the identity operator. The formal solution for μ is

$$\mu = (\mathbf{I} - \mathbf{K})^{-1} f \tag{4}$$

The operator $(\mathbf{I} - \mathbf{K})^{-1}$can be represented by the Neumann series (Hilderbrand, 1965; Kanwal, 1997).

$$\mu = \sum_{m=0}^{\infty} \mathbf{K}^m f \tag{5}$$

where

$$\mathbf{K}^m f \equiv \int_\Gamma K^m(\bar{x}, \bar{y}) f(\bar{y})\, \mathrm{d}s_{\bar{y}} \tag{6}$$

and $K^m(\bar{x}, \bar{y})$ is defined by the following recursive relation

$$K^m(\bar{x}, \bar{y}) = \int_\Gamma K(\bar{x}, \bar{t}) K^{m-1}(\bar{t}, \bar{y})\, \mathrm{d}s_{\bar{t}}, \quad m \geq 1 \tag{7a}$$

$$K^0(\bar{x}, \bar{y}) \equiv 1 \tag{7b}$$

The infinite series solution of μ given by Eq. (5) is called the Neumann series (Hilderbrand, 1965; Kanwal, 1997). The series is absolutely convergent if

$$\sup_{\bar{x} \in \Gamma} \int_\Gamma |K(\bar{x}, \bar{y})|\, \mathrm{d}s_{\bar{y}} < 1$$

The above condition is typically not met by the kernels that appear in linear elasticity. However, it has been shown that the Neumann series representation still holds for linear elasticity. The proof can be found in Parton and Perlin (1982) and Pham (1967). If only traction boundary condition is applied on Γ, it has been shown in Parton and Perlin (1982) that the original series (Eq. (5)) is convergent. For other types of boundary conditions, the original series as shown in Eq. (5) needs to be modified for it to be convergent. The details can be found in chapters 10, 29 and 30 of Parton and Perlin (1982).

The knowledge of $\mu(\bar{x})$ on Γ can then be used to obtain the solution of linear elasticity in Ω. The solution, denoted by $T(\bar{x})$, has the form

$$T(\bar{x}) = \int_\Gamma R(\bar{x}, \bar{y}) \mu(\bar{y})\, \mathrm{d}s_{\bar{y}} \quad \bar{x} \in \Omega, \bar{y} \in \Gamma \tag{8}$$

where $R(\bar{x}, \bar{y})$ is usually closely related to $K(\bar{x}, \bar{y})$. Specific terms of $R(\bar{x}, \bar{y})$ and $K(\bar{x}, \bar{y})$ relevant to linear elasticity problems are given in Section 3. Eq. (8) basically states that the solution at the point of interest is given by a weighted average of μ over the boundary Γ, where the weighting factor is given by the kernel $R(\bar{x}, \bar{y})$. Using the integral operator notation defined above (Eq. (2)), we can write Eq. (8) as

$$T = \mathbf{R}\mu \tag{9}$$

Substituting Eq. (5) into Eq. (9), we obtain the solution for $T(\bar{x})$ in operator notation as

$$T = \mathbf{R}f + \sum_{m=1}^{\infty} \mathbf{R}\mathbf{K}^m f \tag{10}$$

which can be written out more explicitly as

$$T(\bar{x}) = \int_\Gamma R(\bar{x}, \bar{y}) f(\bar{y})\, \mathrm{d}s_{\bar{y}} + \sum_{m=1}^{\infty} \int\int_\Gamma R(\bar{x}, \bar{y}) K^m(\bar{y}, t) f(\bar{t})\, \mathrm{d}s_{\bar{t}}\, \mathrm{d}s_{\bar{y}} \tag{11}$$

In general, it is not possible to evaluate the terms on the right hand side of Eq. (10) or (11) exactly. A numerical scheme is required.

2.2. Probabilistic basis of WBM and its implementation

We need to evaluate the terms on the right hand side of Eq. (10) or (11) in order to obtain $T(\bar{x})$. Walk on the boundary method (WBM) is a numerical scheme that will allow us to compute $T(\bar{x})$ which is the desired solution. It has been shown by Rubinstein (1981) and Sabelfeld (1991) that the terms on the right hand side of Eq. (11) are given by the *expectations of appropriately defined random variables*. The proof of this fact is given in Appendix A. WBM works by estimating the expectation of these random variables through statistical sampling of boundary points. Specifically, the statistical sampling of points on the boundary is done via a random walk on the boundary, Γ

To see how WBM works in more detail, let us begin by noting that the position of a random walker, who starts out at an interior point $\bar{x}$ and lands on the boundary $\bar{y}_i$ $(i \geq 0)$, is a random variable. This random walk is specified by the initialization probability density,$\pi(\bar{x}, \bar{y}_0)$, and the transition probability density, $p(\bar{y}_{i-1}, \bar{y}_i)$. The initialization probability density, $\pi(\bar{x}, \bar{y}_0)$, is defined by noting that $\pi(\bar{x}, \bar{y}_0)\,\mathrm{d}s_{\bar{y}}$, is the probability of a random walker ending up in the neighborhood of point $\bar{y}_0$ given that it started out from point $\bar{x}$. Similarly, $p(\bar{y}_{i-1}, \bar{y}_i)\,\mathrm{d}s_{\bar{y}}$ gives the probability of a random walker moving from point $\bar{y}_{i-1}$ into the neighborhood of point $\bar{y}_i$ on the ith transition. One realization of the random walk on the boundary is depicted in Fig. 1 for three transitions after starting out from some arbitrary point $\bar{x}$ inside the body.

As mentioned earlier, the terms on the right hand side of Eq. (11) are given by the expectations of

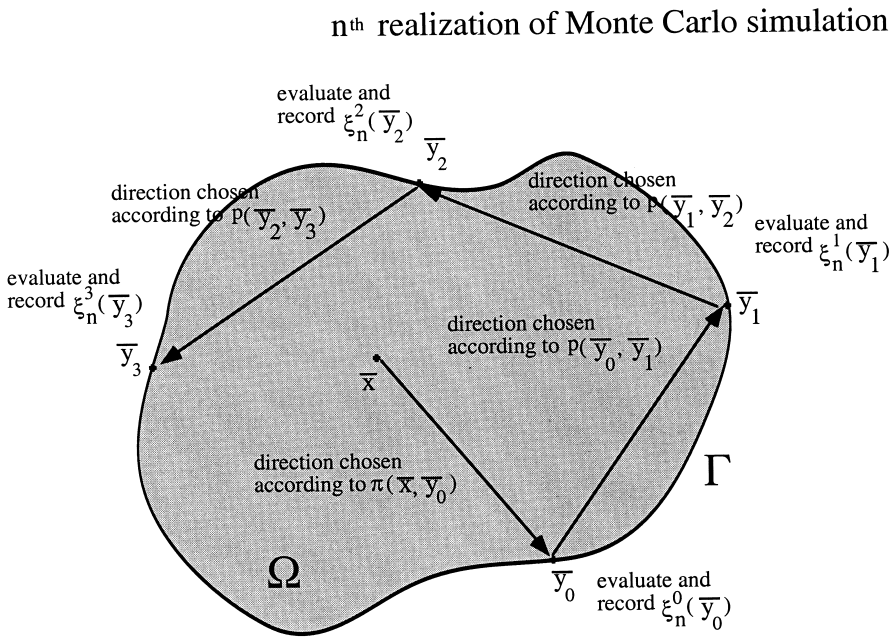

Fig. 1. A schematic illustration of the nth realization of the Monte Carlo simulation of the WBM. The body consists of the domain Ω and the boundary Γ. The initial direction is chosen according to $\pi(\bar{x}, \bar{y}_0)$, initialization probability density, while all subsequent directions are chosen according to $p(\bar{y}_{i-1}, \bar{y}_i)$, transition probability density. Then, the points encountered by the rays are the sample points.

appropriately defined random variables. In this paper, we will adapt the definition used by Sabelfeld (1991), Rubinstein (1981), and Fishman (1996) for these random variables

$$\{\xi^i\}_{i\in I}$$

where I denotes the set of nonnegative integers. Each random variable, ξ^i, is a function of the position of the random walker and is given by the recursive formulae (Sabelfeld, 1991; Rubinstein, 1981; Fishman, 1996)

$$\xi^i = Q^i f(\bar{y}_i), \quad i \geq 0 \tag{12}$$

where

$$Q^i = Q^{i-1}\frac{K(\bar{y}_{i-1}, \bar{y}_i)}{p(\bar{y}_{i-1}, \bar{y}_i)} \tag{13a}$$

$$Q^0 \equiv \frac{R(\bar{x}, \bar{y}_0)}{\pi(\bar{x}, \bar{y}_0)} \tag{13b}$$

and f is the known function on the boundary defined by Eq. (4). It will be shown in Appendix A that the expectation of the random variable, $E(\xi^i)$, $i \geq 1$, is exactly equal to

$$E(\xi^i) = \mathbf{R}\mathbf{K}^i f \tag{14a}$$

and for $i = 0$

$$E(\xi^0) = \mathbf{R} f \tag{14b}$$

Eqs. (14a) and (14b) are exactly the terms on the right hand side of Eq. (10), which, when added together, will give $T(\bar{x})$. Note that $T(\bar{x})$ is given by an infinite series as shown in Eq. (11). In numerical implementations, only a finite number of terms is summed. A way of deciding how many terms are needed is discussed in Appendix B.

By the strong law of large numbers (Billingsley, 1995), the expectation of ξ^i is also given as the following

$$E(\xi^i) = \lim_{N\to\infty}\frac{1}{N}\sum_{n=1}^{N}\xi_n^i \tag{15a}$$

and

$$E(\xi^0) = \lim_{N\to\infty}\frac{1}{N}\sum_{n=1}^{N}\xi_n^0 \tag{15b}$$

where the superscript and the subscript on ξ_n^i are used to denote that ξ_n^i is the ith term of the Neumann series obtained during the nth simulation realization. Based on Eqs. (15a) and (15b), a Monte Carlo procedure can be adopted to estimate $E(\xi^i)$ and $E(\xi^0)$ (Rubinstein, 1981):

1. Generate a sample according to the initialization probability density, $\pi(\bar{x}, \bar{y}_0)$. Random walker moves from point $\bar{x}$ to point $\bar{y}_0$.
2. Evaluate and record ξ_1^0 at point $\bar{y}_0$ according to Eq. (12).

3. Generate a sample according to the transition probability density, $p(\bar{y}_0, \bar{y}_1)$. Random walker moves from point $\bar{y}_0$ to point $\bar{y}_1$
4. Evaluate and record ξ_1^1 at point $\bar{y}_1$ according to Eq. (12)
5. Generate a sample according to the transition probability density, $p(\bar{y}_{i-1}, \bar{y}_i)$. Random walker moves from point $\bar{y}_{i-1}$ to point $\bar{y}_i$.
6. Evaluate and record ξ_1^i at point $\bar{y}_i$ according to Eq. (12), for $i \leq M$
7. Repeat steps 1 through 6 N times, then the solution to $T(\bar{x})$ is estimated by

$$T(\bar{x}) \cong \frac{1}{N} \sum_{i=0}^{M} \sum_{n=1}^{N} \xi_n^i \tag{16}$$

The above Monte Carlo procedure is illustrated schematically in Fig. 1. In the next section, we will show how the WBM can be applied to solving linear elasticity problems.

3. Application of WBM to linear elasticity

Consider a linear elastic body with arbitrary tractions applied on the boundary. The displacement field at any point inside the body Ω can be obtained using integral equations. We will consider antiplane shear, plane strain and 3D problems.

For antiplane shear problems with traction boundary conditions, the resulting equations have the following form (Hartman, 1989)

$$w(\bar{x}) = \int_\Gamma 2g(\bar{x}, \bar{y}) \frac{\partial w(\bar{y})}{\partial \upsilon_{\bar{y}}} \, \mathrm{d}s_{\bar{y}} - \int_\Gamma 2 \frac{\partial g(\bar{x}, \bar{y})}{\partial \upsilon_{\bar{y}}} w(\bar{y}) \, \mathrm{d}s_{\bar{y}}, \quad \bar{x} \in \Gamma \tag{17a}$$

$$w(\bar{x}) - \int_\Gamma g(\bar{x}, \bar{y}) \frac{\partial w(\bar{y})}{\partial \upsilon_{\bar{y}}} \, \mathrm{d}s_{\bar{y}} = - \int_\Gamma \frac{\partial g(\bar{x}, \bar{y})}{\partial \upsilon_{\bar{y}}} w(\bar{y}) \, \mathrm{d}s_{\bar{y}}, \quad \bar{x} \in \Omega \tag{17b}$$

where $w(\bar{x})$ is the out of plane displacement and it is defined as the displacement in the direction perpendicular to the x–y plane at $\bar{x}$ (see Fig. 2), $g(\bar{x}, \bar{y})$ is the out of plane displacement at $\bar{x}$ due to a point force at $\bar{y}$ (Hartman, 1989), i.e.,

$$g(\bar{x}, \bar{y}) = -\frac{1}{2\pi} \ln(r)$$

$$r = |\bar{y} - \bar{x}|.$$

Also, the shear modulus has been set to 1 for the convenience of computation, $\partial w / \partial \upsilon_{\bar{y}}$ is equal to the specified traction on the boundary and $\upsilon_{\bar{y}}$ is the unit normal vector at point $\bar{y}$. Note that Eq. (17a) holds for points on the boundary of the body and Eq. (17b) holds for points inside the body.

Suppose we are interested in finding the displacement value at points inside the body, then by comparing Eq. (17a) to Eq. (1) and Eq. (17b) to Eq. (8), we find in antiplane shear problems that

$$\mu = w \tag{18a}$$

$$K_s = -2 \frac{\partial g}{\partial \upsilon_{\bar{y}}} \tag{18b}$$

$$f = \int_\Gamma 2g \frac{\partial w}{\partial \upsilon_{\bar{y}}} \, \mathrm{d}s_{\bar{y}} \tag{18c}$$

$$R_s = \left(\frac{1}{2}\right) K_s \tag{18d}$$

and

$$T = w - \int_\Gamma g \frac{\partial w}{\partial \upsilon_{\bar{y}}} \, \mathrm{d}s_{\bar{y}} \tag{18e}$$

where the subscript s in K_s and R_s is used to emphasize that they are the kernels corresponding to the antiplane shear case. Since $\partial w/\partial \upsilon_{\bar{y}}$ is the given traction, $\int_\Gamma g \, \partial w/\partial \upsilon_{\bar{y}} \, \mathrm{d}s_{\bar{y}}$ can be evaluated explicitly. Hence, after T is estimated based on the Monte Carlo procedure described in the previous section, we can solve for w using Eq. (18e).

The next task is to find a random walk on the boundary to simulate, i.e., determine what initialization probability density, $\pi(\bar{x}, \bar{y}_0)$, and transition probability density, $p(\bar{y}_{i-1}, \bar{y}_i)$, to use. It will be shown in Appendix C that we can set $p(\bar{y}_{i-1}, \bar{y}_i) = |K_s(\bar{y}_{i-1}, \bar{y}_i)|$ and $\pi(\bar{x}, \bar{y}_0) = |R_s(\bar{x}, \bar{y}_0)|$ for convex domains. Modifications to $\pi(\bar{x}, \bar{y}_0)$ and $p(\bar{y}_{i-1}, \bar{y}_i)$ based on $|R_s(\bar{x}, \bar{y}_0)|$ and $|K_s(\bar{y}_{i-1}, \bar{y}_i)|$ for nonconvex domains are given in Appendix C (see Eqs. (C6a) and (C6b)). A method of generating random walk samples according to $|R_s(\bar{x}, \bar{y}_0)|$ and $|K_s(\bar{y}_{i-1}, \bar{y}_i)|$ for convex and nonconvex domains is also given in Appendix C. Of course, we can choose other $p(\bar{y}_{i-1}, \bar{y}_i)$s and $\pi(\bar{x}, \bar{y}_0)$s, but these other choices may lead to large variances in ξ^i, therefore, requiring a large number of samples to achieve the desired error tolerance as shown in Section 5 of the paper. It turns out that in the antiplane shear problems $p(\bar{y}_{i-1}, \bar{y}_i) = |K_s(\bar{y}_{i-1}, \bar{y}_i)|$ and $\pi(\bar{x}, \bar{y}_0) = |R_s(\bar{x}, \bar{y}_0)|$ are the optimal choice (Mikhailov, 1992). The subject of finding the

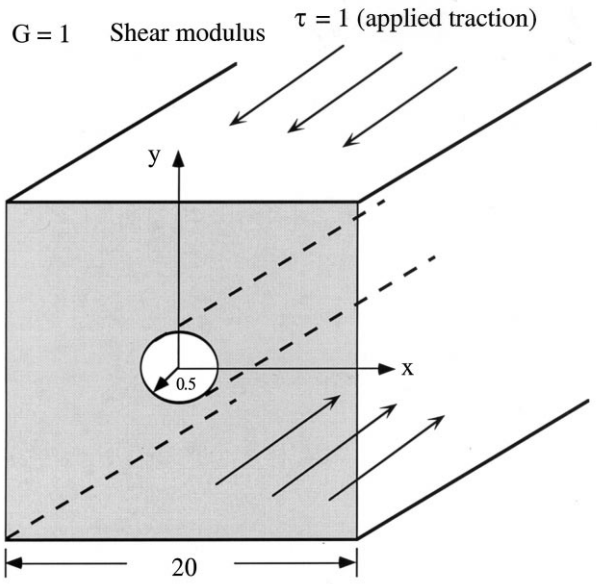

Fig. 2. Antiplane shear example problem: A linear elastic body with a square cross section of length 20 containing a centrally located circular hole of radius 0.5, is being loaded by uniform shear tractions on the top and bottom faces. Also shown is the coordinate system used in the problem with its origin located at the center of the hole.

optimal $p(\bar{y}_{i-1}, \bar{y}_i)$ and $\pi(\bar{x}, \bar{y}_0)$ is called 'importance sampling' in Monte Carlo simulation literatures (e.g. Mikhailov, 1992; Ross, 1997). We will not discuss importance sampling here.

Using the choice of $p(\bar{y}_{i-1}, \bar{y}_i) = |K_s(\bar{y}_{i-1}, \bar{y}_i)|$ and $\pi(\bar{x}, \bar{y}_0) = |R_s(\bar{x}, \bar{y}_0)|$ for our random walk on the boundary, the random variable defined in Eqs. (12), (13a) and (13b) for convex domains becomes

$$\xi^i = (-1)^i f(\bar{y}_i), \quad i \geq 0 \tag{19}$$

Using the Monte Carlo procedure described in Section 2.2, the solution to the antiplane shear problems, $T(\bar{x})$, is estimated by

$$T(\bar{x}) \cong \frac{1}{N} \sum_{i=0}^{M} \sum_{n=1}^{N} (-1)^i f_n(\bar{y}_i) \tag{20a}$$

where M denotes the number of terms kept in the Neumann series and N denotes the total number of samples generated. The Monte Carlo procedure remains unchanged for nonconvex domains, except that Eq. (20a) is now given as follows

$$T(\bar{x}) \cong \frac{1}{N} \sum_{i=0}^{M} \sum_{n=1}^{N} (-1)^i f_n(\bar{y}_i) q(\bar{y}_i) \tag{20b}$$

where $q(\bar{y}_i)$ is the number of intersection with Γ of the ray $(\bar{y}_i - \bar{y}_{i-1})$ excluding the point $\bar{y}_{i-1}$

We can also formulate plane and 3D problems with known boundary tractions in terms of integral equations. The formulation is very similar to that of antiplane shear problems. The integral equations are (Hartman, 1989)

$$u_i(\bar{x}) = 2 \int_\Gamma \left[U_{ij}(\bar{x}, \bar{y}) t_j(\bar{y}) - T_{ij}(\bar{x}, \bar{y}) u_j(\bar{y}) \right] \mathrm{d}s_{\bar{y}}, \quad \bar{x} \in \Gamma \tag{21a}$$

$$u_i(\bar{x}) - \int_\Gamma U_{ij}(\bar{x}, \bar{y}) t_j(\bar{y}) \, \mathrm{d}s_{\bar{y}} = - \int_\Gamma T_{ij}(\bar{x}, \bar{y}) u_j(\bar{y}) \, \mathrm{d}s_{\bar{y}}, \quad \bar{x} \in \Omega \tag{21b}$$

where u_i denotes the ith component of the displacement vector in the jth direction, $U_{ij}(\bar{x}, \bar{y})$ denotes the kernel that gives the displacement in the ith direction at point $\bar{x}$ due to a unit point force in the jth direction at point $\bar{y}$, t_j denote the jth component of the traction vector, and $T_{ij}(\bar{x}, \bar{y})$ denotes the kernel that gives the traction in the ith direction at point $\bar{x}$ due to a unit point force in the jth direction at point $\bar{y}$. The summation convention is used in Eqs. (21a) and (21b), i.e., for plane problems i and j run from 1 to 2 and for 3D problems i and j run from 1 to 3. Note that the unknown u_i is a vector instead of a scalar as in the antiplane shear case. Also note that the kernels U_{ij} and R_{ij} are both $n \times n$ matrices instead of scalars as in the antiplane shear case. However, these differences do not make the WBM anymore complicated than in the antiplane shear case. Explicit expressions for the kernels $U_{ij}(\bar{x}, \bar{y})$ and $T_{ij}(\bar{x}, \bar{y})$ are given below for completeness (Hartman, 1989).

$$U_{ij}(\bar{x}, \bar{y}) = \frac{1}{16\pi G(1-\nu) r} \left[(3 - 4\nu)\delta_{ij} + r_{,i} r_{,j} \right] \quad \text{3D} \tag{22a}$$

$$U_{ij}(\bar{x}, \bar{y}) = \frac{1}{8\pi G(1-\nu)} \left[(3 - 4\nu) \ln\left(\frac{1}{r}\right) \delta_{ij} + r_{,i} r_{,j} \right] \quad \text{2D} \tag{22b}$$

$$T_{ij}(\bar{x},\bar{y}) = \frac{-1}{4\alpha\pi(1-\nu)r^{\alpha}}\left[\frac{\partial r}{\partial \nu}\left((1-2\nu)\delta_{ij}+\beta r_{,i}r_{,j}\right)-(1-2\nu)\left\{r_{,i}\nu_j(\bar{y})-r_{,j}\nu_i(\bar{y})\right\}\right] \tag{23}$$

where $\alpha = 1$, $\beta = 2$ in 2D, $\alpha = 2$, $\beta = 3$ in 3D, δ_{ij} is the Kronecker delta, G is the shear modulus, ν is the Poisson's ratio, $r = |\bar{x}-\bar{y}|$ is the distance between point $\bar{x}$ and $\bar{y}$, $r_{,i} = (y_i - x_i)/r$, and $\nu_i(\bar{y})$ is the ith component of the unit normal vector at point $\bar{y}$.

As in the antiplane shear problems, we can make similar correspondences of Eq. (21a) to Eq. (1) and (21b) to Eq. (8). We find that:

$$\mu = u_i$$

$$K = -2T_{ij}$$

$$f = 2\int_{\Gamma} U_{ij}(\bar{x},\bar{y})t_j(\bar{y})\,\mathrm{d}s_{\bar{y}}$$

$$R = -T_{ij}$$

$$T = u_i - \int_{\Gamma} U_{ij}(\bar{x},\bar{y})t_j(\bar{y})\,\mathrm{d}s_{\bar{y}}$$

Note that the integral $\int_{\Gamma} U_{ij}(\bar{x},\bar{y})t_j(\bar{y})\,\mathrm{d}s_{\bar{y}}$ can be evaluated explicitly since the boundary traction is known and hence, we can solve for the unknown displacement.

Our next task, as in the antiplane shear case, is to identify an appropriate random walk to simulate. It was relatively simple to identify the appropriate random walk in the antiplane shear case, since the kernels, $|K_s(\bar{y}_i,\bar{y}_{i-1})|$ and $|R_s(\bar{x},\bar{y}_0)|$, lent themselves to probabilistic interpretations easily, as shown in Appendix C. Here, the kernels $U_{ij}(\bar{x},\bar{y})$ and $T_{ij}(\bar{x},\bar{y})$ cannot be interpreted easily in a probabilistic sense. Therefore, we will again set $p(\bar{y}_{i-1},\bar{y}_i) = |K_s(\bar{y}_{i-1},\bar{y}_i)|$ for the transition probability density, and $\pi(\bar{x},\bar{y}_0) = |R_s(\bar{x},\bar{y}_0)|$ for the initialization probability density for convex domains and for nonconvex domains we will use the modifications given in Appendix C (Eq. (C6a,b)). Note that the choice made for the transition and initialization probability densities is not the optimal choice based on importance sampling (Mikhailov, 1992). However, the current choice does have some nice features: (1) it is very easy to simulate numerically and (2) its functional behavior is quite similar to that of the kernels which will limit the variance, hence, the error.

Specializing to plane and 3D problems, the random variable, or random vector in this case, defined by Eqs. (12)–(13a) now becomes

$$\xi_n^i = Q_{nk}^i f_k(\bar{y}_i), \quad i \geq 0 \tag{24}$$

where

$$Q_{nk}^i = \frac{Q_{nm}^{i-1}\left[-2T_{mk}(\bar{y}_{i-1},\bar{y}_i)\right]}{|K_s(\bar{y}_{i-1},\bar{y}_i)|}, \quad i \geq 1 \tag{25a}$$

and

$$Q_{nm}^0 = \frac{-T_{nm}(\bar{x},\bar{y}_0)}{|R_s(\bar{x},\bar{y}_0)|}, \quad i = 0 \tag{25b}$$

Note that subscripts in Eq. (24) through Eq. (25b) denote components of a vector or a matrix, not simulation runs as in Eqs. (20a) and (20b). The same Monte Carlo procedure given in Section 2.2 applies for plane strain and 3D problems. The components of the unknown vector T_n is estimated as given below

$$T_n(\bar{x}) \cong \frac{1}{N}\sum_{i=0}^{M}\sum_{m=1}^{N}\left(\xi_n^i\right)_m \tag{26}$$

For nonconvex domains, the Monte Carlo procedure remains the same, except that Eqs. (25a) and (25b) become

$$Q_{nk}^i = \frac{q(\bar{y}_i)Q_{nm}^{i-1}\left[-2T_{mk}(\bar{y}_{i-1},\bar{y}_i)\right]}{|K_s(\bar{y}_{i-1},\bar{y}_i)|}, \quad i \geq 1$$

and

$$Q_{nm}^0 = \frac{-q(\bar{y}_0)T_{nm}(\bar{x},\bar{y}_0)}{|R_s(\bar{x},\bar{y}_0)|}, \quad i = 0$$

Next, we apply the WBM to solve three example problems in linear elasticity.

4. Numerical examples

The WBM is applied to the following three numerical examples: (1) a square region containing a centrally located circular hole with uniform antiplane shear traction applied on the top and bottom faces as shown in Fig. 2, (2) a plane strain problem of a square region containing a centrally located circular hole with uniform tension being applied on the top and bottom faces as shown in Fig. 3, and (3) a 3D problem of a cubic region containing a centrally located spherical cavity with uniform tension being applied on the top and bottom faces as shown in Fig. 4

4.1. Antiplane shear problem

The problem solved is a square region containing a circular hole with uniform antiplane shear traction applied on the top and bottom faces. This is illustrated in Fig. 2 along with the coordinate system and the dimensions of the body used in computation. Note that the value of traction and shear modulus is set to unit magnitude for the convenience of computation. The numerical results are tabulated in Table 1 along with the displacement values obtained from the analytical solution of a circular hole within an infinite domain. The comparison made here between the numerical solution and the exact solution is valid as long as the points are not too far away from the circular hole, since the square region is approximately 20 times larger than the circular hole. All numerical solutions are obtained with 20,000 samples and using one term in the Neumann series, in short, 20,000(1). The errors are computed according to Eq. (30). Note that the numerical solution compares favorably with the analytical solution, except when we move farther away from the circular hole as shown by the last point in Table 1, which is to be expected.

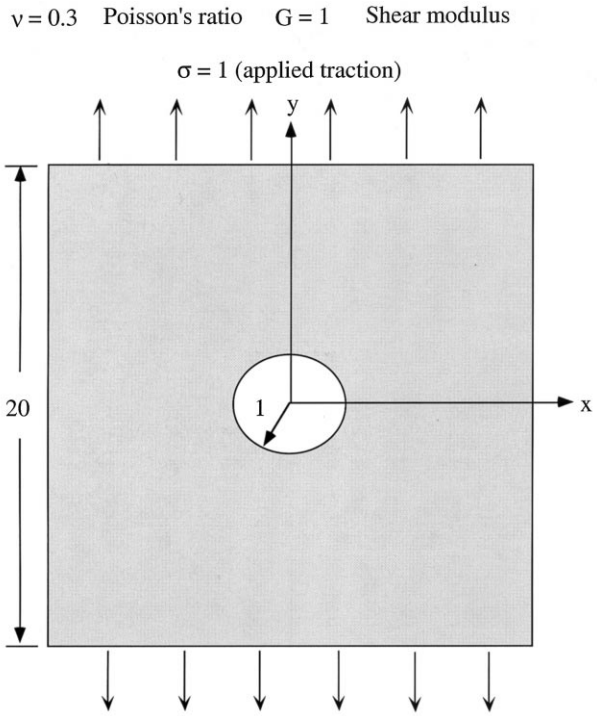

Fig. 3. Plane strain example problem: A linear elastic body of square cross section of length 20 containing a centrally located circular hole of radius 1.0, is being loaded by uniform tension on the top and bottom faces. Also shown is the coordinate system used in the problem with its origin located at the center of the hole.

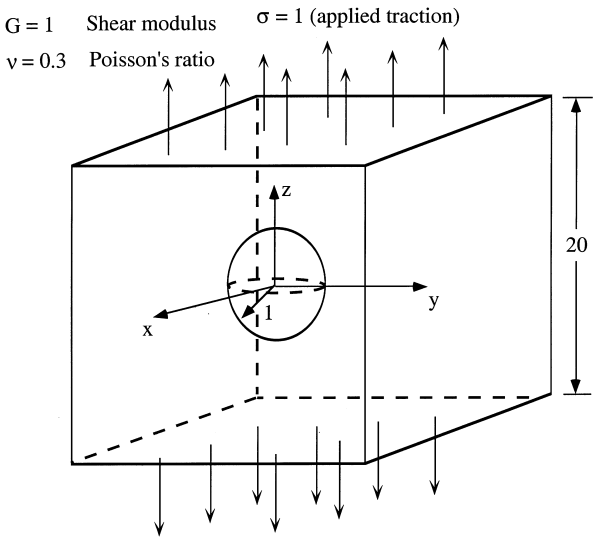

Fig. 4. 3D elasticity example problem: A cubic linear elastic body of side length 20 containing a centrally located spherical cavity of radius 1.0, is being loaded by uniform tension on the top and bottom faces. Also shown is the coordinate system used in the problem with its origin located at the center of the cavity.

Table 1
Comparison between numerical and analytical solution for antiplane shear problem

x	y	$w_{\text{numerical}}$	$w_{\text{analytical}}$
0.55	0.55	0.78 ± 0.07	0.78
0.6	0.6	0.82 ± 0.07	0.81
0.65	0.433	0.61 ± 0.063	0.61
1.2	0.5	0.58 ± 0.04	0.57
2	3	3.00 ± 0.04	3.06

4.2. Plane strain problem

The example problem solved is a square region containing a circular hole being loaded by uniform far-field tension of unit magnitude. This is illustrated in Fig. 3 along with the coordinate system and the dimensions of the body. Numerical and analytical results are tabulated in Table 2 for comparison. As in the previous section, the infinite domain analytical results are used. The numerical results are obtained with 400,000(1). Again, the numerical solution compares favorably with the analytical solution.

4.3. 3D problem

The example problem is a cubic region containing a spherical cavity being loaded by uniform tension of unit magnitude. It is illustrated in Fig. 4 along with the coordinate system and the dimensions of the body. The numerical solution from the WBM is compared to the solution obtained via the finite element method. This is shown in Table 3 below. The WBM results compare well with the results via the finite element method. The WBM results are obtained with 400,000(1).

Note that in all the three example problems only one term is used in the Neumann series. A statistical procedure based on hypothesis testing is developed to determine the number of terms needed in the Neumann series. It has been applied to all the three problems. Details of the procedure can be found in Appendix B. Based on the statistical procedure, we have found that, in all three problems, additional terms do not contribute much to the summation and their inclusions will result in greater sampling errors in the final solution.

It was also noted that the number of samples depends on a preset tolerance level of sampling errors and the variance associated with the random variable; a large variance implies a large number of samples is required to achieve the preset error tolerance. For each of the three example problems approximately the same level of sampling error tolerance has been used, but the variance in the antiplane shear problem is smaller than in the plane strain and 3D problems. This is to be expected

Table 2
Comparison between numerical and analytical solution for plane strain problem

gx	y	u_1 (numerical)	u_2 (numerical)	u_1 (analytical)	u_2 (analytical)
0	1.5	0	1.09 ± 0.096	0	1.08
0	1.6	0	1.11 ± 0.093	0	1.09
0	1.7	0	1.13 ± 0.091	0	1.10
0	2.0	0	1.20 ± 0.082	0	1.15
0	2.5	0	1.27 ± 0.061	0	1.24

Table 3
Comparison between WBM and FEM solution for 3D problem

x	y	z	u_1 & u_2 (WBM)	u_3 (WBM)	u_1 & u_2 (FEM)	u_3 (FEM)
0	0	1.521	0	0.80 ± 0.01	0	0.83
0	0	1.677	0	0.83 ± 0.01	0	0.85
0	0	1.873	0	0.90 ± 0.01	0	0.89
0	0	2.117	0	0.99 ± 0.01	0	0.95

since the optimal sampling scheme is used for the antiplane shear case. Hence, only 20,000 samples were needed in the antiplane shear problem as compared to 400,000 samples in the plane strain and 3D problems. In the next section, an explicit formula is given for computing the sampling error.

5. Error analysis

There are two sources of error associated with the WBM. The first source of error is due to truncating the infinite series (Eq. (5)). The second source, called sampling error, arises due to variance associated with the random variable, ξ^i. In general, the first source of error cannot be determined explicitly. We must perform convergence tests empirically to determine the appropriate number of terms to keep. Once the appropriate number of terms has been determined via the procedure described in Appendix B, the sampling error becomes the major source of error in WBM. In this section we will present the expression necessary for estimating the second source of error.

We know from the central limit theorem that for large values of N

$$\sqrt{N}\frac{(\bar{X}-\theta)}{\sqrt{\mathrm{Var}(\xi^i)}} \sim \mathrm{Normal}(0,\,1) \tag{27}$$

where $\sim$Normal(0, 1) means 'is approximately distributed as a unit normal', $\bar{X}$ is given by $\frac{1}{N}\sum_{n=1}^{N}\xi_n^i$, and θ is given by $\int\int_\Gamma R(\bar{x},\,\bar{y})K^i(\bar{y},\,\bar{t})f(\bar{t})\,\mathrm{d}s_{\bar{t}}\,\mathrm{d}s_{\bar{y}}$ for $i \geq 1$, and is given by $\int_\Gamma R(\bar{x},\,\bar{y})f(\bar{y})\,\mathrm{d}s_{\bar{y}}$ for $i = 0$. Define Z to be a unit normal random variable. Let z_α be such that the probability of $Z > z_\alpha$ is

$$P\{Z > z_\alpha\} = \alpha$$

where α is any number between zero and one. It follows from the symmetry of the unit normal density function about the origin that

$$P\left\{\bar{X} - z_{\alpha/2}\frac{\sqrt{\mathrm{Var}(\xi^i)}}{\sqrt{N}} < \theta < \bar{X} + z_{\alpha/2}\frac{\sqrt{\mathrm{Var}(\xi^i)}}{\sqrt{N}}\right\} \cong 1-\alpha \tag{28}$$

In other words, the probability that the exact solution, θ, will lie within the interval $\bar{X} \pm z_{\alpha/2}\sqrt{\mathrm{Var}(\xi^i)}/\sqrt{N}$ is $1-\alpha$. Values of z_α can be obtained from tables of Spiegel (1995) for different values of α or confidence. In general, we do not know $\mathrm{Var}(\xi^i)$. However, $\mathrm{Var}(\xi^i)$ can be estimated using (Spiegel, 1995)

$$S^2 = \frac{1}{N-1}\sum_{n=1}^{N}\left(\xi_n^i - \bar{X}\right)^2 \tag{29}$$

By Slutsky's theorem (Billingsley, 1995), if we replace $\sqrt{\mathrm{Var}(\xi^i)}$ in Eq. (28) by S we still have a random variable that is distributed approximately as unit normal for large N. Therefore, the interval can be estimated as before and is

$$\bar{X} \pm \frac{z_{\alpha/2} S}{\sqrt{N}} \tag{30}$$

for any given level of confidence, α. Eq. (30) is the desired result for estimating the sampling error. All errors in the example problems are estimated with $z_{\alpha/2} = 1$.

6. Conclusions

A Monte Carlo method, called walk on the boundary method (WBM), for solving linear elasticity problems is carried out. The governing integral equations are based on the BEM formulation. The resulting integral equations are solved via the WBM. This method does not require any kind of meshing. Thus, the method can be very well suited for linear elasticity problems involving a large number of microstructures in 3D, where meshing can be particularly taxing on computing resources. Also, when one is interested in obtaining solutions at a few points in an elastic body, the WBM is a very efficient method since with the WBM, solutions can be obtained only at points of interest. Furthermore, error estimates for WBM is very easy to obtain and is given by Eq. (30).

The WBM is developed in detail for antiplane shear problems, plane strain problems and 3D problems with traction boundary conditions. The developed schemes are then applied to three sample problems — (1) square body containing a circular hole undergoing antiplane shear (2) square body with a circular hole under uniform traction, and (3) a cube containing a spherical cavity being loaded by uniform tension. The numerical results in the first two problems agree well with the analytical solutions. For the third problem, a comparison between the WBM and the FEM is made, and a favorable comparison is obtained. Overall, the numerical results are in reasonable agreement with the exact and FEM solutions, hence demonstrating the feasibility of the WBM, at least for problems with traction boundary conditions.

The proposed WBM is not intended as a replacement for FEM nor BEM. At its current stage of development for linear elasticity problems, it is definitely not as versatile as FEM and BEM. In order to make WBM more useful, there are some issues associated with WBM that need to be addressed. These issues are: (1) stress calculations, (2) displacement and mixed boundary conditions, and (3) efficiency of the random walk simulation, i.e., we need to find a better initialization and transition probability density to use in the case of plane and 3D problems. However, as a feasibility study, it is demonstrated that WBM is a viable method for solving linear elasticity problems, and by resolving the aforesaid issues it is possible that WBM can become more versatile and useful in the future.

Acknowledgements

The idea of solving linear elasticity problems via probabilistic methods originated from a seminar given in the Department of Theoretical and Applied Mechanics by Prof. M. Grigoriu.

Appendix A

We will prove here the claim that

$$E(\xi^i) = \int\int_\Gamma R(\bar{x}, \bar{y}) K^i(\bar{y}, \bar{t}) f(\bar{t})\, \mathrm{d}s_{\bar{t}}\, \mathrm{d}s_{\bar{y}}$$

and

$$E(\xi^0) = \int_\Gamma R(\bar{x}, \bar{y}) f(\bar{y})\, \mathrm{d}s_{\bar{y}}$$

Let us begin by considering a specific case, i.e., $i = 2$. For $i = 2$, ξ^2 according to Eqs. (13a), (13b), (14a) and (14b) is given below

$$\xi^2 = \frac{R(\bar{x}, \bar{y}_0)}{\pi(\bar{x}, \bar{y}_0)} \frac{K(\bar{y}_0, \bar{y}_1)}{p(\bar{y}_0, \bar{y}_1)} \frac{K(\bar{y}_1, \bar{y}_2)}{p(\bar{y}_1, \bar{y}_2)} f(\bar{y}_2) \tag{A1}$$

To compute the expectation of the above random variable, we must integrate over all possible paths of the random walk weighted by the probability density given below

$$\pi(\bar{x}, \bar{y}_0) p(\bar{y}_0, \bar{y}_1) p(\bar{y}_1, \bar{y}_2) \tag{A2}$$

Therefore, the expectation, $E(\xi^2)$, is computed as

$$\int\int\int_\Gamma \frac{R(\bar{x}, \bar{y}_0)}{\pi(\bar{x}, \bar{y}_0)} \frac{K(\bar{y}_0, \bar{y}_1)}{p(\bar{y}_0, \bar{y}_1)} \frac{K(\bar{y}_1, \bar{y}_2)}{p(\bar{y}_1, \bar{y}_2)} f(\bar{y}_2) \pi(\bar{x}, \bar{y}_0) p(\bar{y}_0, \bar{y}_1) p(\bar{y}_1, \bar{y}_2)\, \mathrm{d}s_{\bar{y}_0}\, \mathrm{d}s_{\bar{y}_1}\, \mathrm{d}s_{\bar{y}_2} \tag{A3}$$

Eq. (A3) can be simplified to become

$$\int\int\int_\Gamma R(\bar{x}, \bar{y}_0) K(\bar{y}_0, \bar{y}_1) K(\bar{y}_1, \bar{y}_2) f(\bar{y}_2)\, \mathrm{d}s_{\bar{y}_0}\, \mathrm{d}s_{\bar{y}_1}\, \mathrm{d}s_{\bar{y}_2} \tag{A4}$$

Note that

$$K^2(\bar{y}_0, \bar{y}_2) = \int_\Gamma K(\bar{y}_0, \bar{y}_1) K(\bar{y}_1, \bar{y}_2)\, \mathrm{d}s_{\bar{y}_1} \tag{A5}$$

according to Eq. (3). Hence, Eq. (A4) can be rewritten as

$$E(\xi^2) = \int\int_\Gamma R(\bar{x}, \bar{y}_0) K^2(\bar{y}_0, \bar{y}_2) f(\bar{y}_2)\, \mathrm{d}s_{\bar{y}_0}\, \mathrm{d}s_{\bar{y}_2} \tag{A6}$$

which is exactly the third term in Eq. (5). Following the same procedure as shown above, we can easily prove the claim made in the beginning of the Appendix for other values of i.

Appendix B

In this Appendix, we will develop a statistical test for determining whether the ith term in the

Neumann series (Eq. (10) or Eq. (11)) is significantly greater than zero. We will then be able to decide whether we should keep the ith term, or truncate the series at the ith term.

We start by noting that according the central limit theorem (Billingsley, 1995),

$$\frac{\sqrt{n}\left[E\left(\xi^i\right)-\mu_i\right]}{\sigma_i}\sim N(0,1),\quad i\geq 0 \tag{B1}$$

where n is the number of samples, $E(\xi^i)$ can be estimated from Eqs. (15a) and (15b), μ_i (unknown) is the actual value of the ith term of the Neumann series and σ_i is the standard deviation of the random variable $E(\xi^i)$. The symbol, $\sim N(0,1)$, means that the random variable, $\sqrt{n}[E(\xi^i)-\mu_i]/\sigma_i$, is distributed as a normal random variable with zero mean and unit variance. A random variable with such a distribution is also called the standard normal variable and its distribution is called the standard normal distribution. The standard deviation, σ_i, can be estimated by the following formula (Spiegel, 1995)

$$\sigma_i^2\cong\frac{1}{n}\sum_{m=1}^{n}\left(\xi_m^i\right)^2-\left(E\left(\xi^i\right)\right)^2 \tag{B2}$$

We can develop a statistical test based on Eq. (B1). Let us begin with the hypothesis that $\mu_i=0$. According to Eq. (B1), the hypothesis implies that

$$\frac{\sqrt{n}\left[E\left(\xi^i\right)\right]}{\sigma_i}\sim N(0,1) \tag{B3}$$

Since $E(\xi^i)$ provides an estimate for μ_i, we would expect Eq. (B3) to be significantly greater than zero if μ_i itself is also significantly greater than zero. We can provide a quantitative measure of this significance by utilizing the fact that $\sqrt{n}[E(\xi^i)]/\sigma_i$'s distribution is known. To quantify this significance, we start by computing the following probability

$$P\left(\left|\frac{\sqrt{n}\left[E\left(\xi^i\right)\right]}{\sigma_i}\right|>z_{\alpha/2}\right)=\alpha \tag{B4}$$

where $z_{\alpha/2}$ is defined to be the point at which the area under the density of the standard normal variable to its right is equal to $\alpha/2$.

Now, suppose $\alpha=0.01,\quad z_{0.005}=2.57$, then Eq. (B4) is saying that $|\sqrt{n}[E(\xi^i)]/\sigma_i|$ is greater than 2.57, which occurs by pure chance only one percent of the time under the hypothesis that μ_i is equal to zero. Therefore, if $|\sqrt{n}[E(\xi^i)]/\sigma_i|$ is greater than 2.57 then it is unlikely that this has occurred by pure chance, hence, we have to reject the hypothesis that μ_i is equal to zero. In statistical terms, we call $1-\alpha$ the significance level of the test. For the above scenario, we would say that we have rejected the hypothesis

Table B1
Test statistic results for 3D sample problem

x	y	z	$\left\lvert\frac{\sqrt{n}E(\xi_1^1)}{\sigma_1^1}\right\rvert$	$\left\lvert\frac{\sqrt{n}E(\xi_2^1)}{\sigma_2^1}\right\rvert$	$\left\lvert\frac{\sqrt{n}E(\xi_3^1)}{\sigma_3^1}\right\rvert$	$\left\lvert\frac{\sqrt{n}E(\xi_3^2)}{\sigma_3^2}\right\rvert$
0.0	0.0	1.521	1.28	0.113	16.5	1.72
0.0	0.0	1.677	1.27	0.251	14.9	2.10
0.0	0.0	1.873	1.67	0.780	16.5	0.52
0.0	0.0	2.117	1.09	0.830	19.8	0.53

that μ_i is equal to zero at a 99 percent significance level. Based on the above statistical test, we can use the following procedure to determine whether we should keep the ith term in the Neumann series or not:

1. Compute $|\sqrt{n}[E(\xi^i)]/\sigma_i|$.
2. If $|\sqrt{n}[E(\xi^i)]/\sigma_i|$ is greater than 2.57, keep the ith term.
3. Repeat test for latter terms until $|\sqrt{n}[E(\xi^m)]/\sigma_m|(m > i)$ is less than 2.57, then truncate series at mth term.

The above procedure can be easily implemented within a program based on the WBM. Results for the 3D example problem are tabulated below in Table B1. The results shown in Table B1 are obtained with 400,000 samples. Note that the subscript associated with ξ_j^i and σ_j^i refers to the jth component of the ith term solution vector in the Neumann series and its standard deviation, respectively. According to Table B1, we see that $E(\xi_1^1)$, $E(\xi_2^1)$ and $E(\xi_3^2)$ are not significantly greater than 0. Only $E(\xi_3^1)$ is significantly greater than zero. Therefore, in this case, only one term is needed in the Neumann series.

Appendix C

In this Appendix, we will discuss the probabilistic interpretations of $|R_s(\bar{x}, \bar{y}_0)|$ and $|K_s(\bar{y}_{i-1}, \bar{y}_i)|$, hence, showing the reason why we can set $p(\bar{y}_{i-1}, \bar{y}_i) = |K_s(\bar{y}_{i-1}, \bar{y}_i)|$ and $\pi(\bar{x}, \bar{y}_0) = |R_s(\bar{x}, \bar{y}_0)|$ for antiplane shear problems. We will first focus on convex regions (e.g. circular bodies), then we will consider nonconvex regions (e.g. multiply connected bodies). Also, we will discuss how to generate random walk samples according to $\pi(\bar{x}, \bar{y}_0)=|R_s(\bar{x}, \bar{y}_0)|$ and $p(\bar{y}_{i-1}, \bar{y}_i) = |K_s(\bar{y}_{i-1}, \bar{y}_i)|$

To begin, let us examine $|K_s(\bar{y}_{i-1}, \bar{y}_i)|$ in more detail. For the antiplane shear problems, $|K_s(\bar{y}_{i-1}, \bar{y}_i)|$ can be written as below

$$|K_s(\bar{y}_{i-1}, \bar{y}_i)| = \frac{1}{\pi}\left\{ \frac{(y_i^1 - y_{i-1}^1)v_1}{(y_i^1 - y_{i-1}^1)^2+(y_i^2 - y_{i-1}^2)^2} + \frac{(y_i^2 - y_{i-1}^2)v_2}{(y_i^1 - y_{i-1}^1)^2+(y_i^2 - y_{i-1}^2)^2} \right\} \tag{C1}$$

where (y_i^1, y_i^2) and (y_{i-1}^1, y_{i-1}^2) are the x and y components of the point $\bar{y}_i$ and $\bar{y}_{i-1}$, respectively, and v_1 and v_2 are the x and y components of the unit normal associated with the point $\bar{y}_i$. Eq. (C1) can be written as

$$|K_s(\bar{y}_{i-1}, \bar{y}_i)| = \frac{1}{\pi}\left\{ \frac{(\bar{y}_i - \bar{y}_{i-1}) \bullet \bar{v}}{|\bar{y}_i - \bar{y}_{i-1}|^2} \right\} \tag{C2}$$

where $\bullet$ denotes dot product. By invoking the definition of dot product, Eq. (C2) becomes

$$|K_s(\bar{y}_{i-1}, \bar{y}_i)| = \frac{1}{\pi}\frac{\cos(\theta)}{|\bar{y}_i - \bar{y}_{i-1}|} \tag{C3}$$

where θ denotes the angle between the vector $(\bar{y}_i - \bar{y}_{i-1})$ and the unit normal, $\bar{v}$, at point $\bar{y}_i$. In this form, Eq. (C3) can easily be given a probabilistic interpretation.

Let us now consider the probability of the event that the random walk, after leaving from $\bar{y}_{i-1}$, ends up in the neighborhood of $\bar{y}_i$. The probability of this event occurring is given by $p(\bar{y}_i, \bar{y}_{i-1})\mathrm{d}s$ where $\mathrm{d}s$ denotes an arc element of the boundary. Suppose that the direction at $\bar{y}_{i-1}$ is chosen from a uniform distribution of angles between $(0, \pi)$ and $\bar{y}_i$ is the point where the straight trajectory strikes the boundary, then we can obtain an explicit expression for the probability of the event as

$$p(\bar{y}_{i-1}, \bar{y}_i)ds = \frac{1}{\pi}\frac{\cos(\theta_i)ds}{|\bar{y}_i - \bar{y}_{i-1}|} \tag{C4}$$

Note that $d\omega = \cos(\theta)ds/|\bar{y}_i - \bar{y}_{i-1}|$ is just the angle subtended by the arc element ds when viewed from $\bar{y}_{i-1}$. By comparing Eq. (C4) to Eq. (C3), we see that we can identify $|K_s(\bar{y}_{i-1}, \bar{y}_i)|$ with $p(\bar{y}_i, \bar{y}_{i-1})$. Similarly, the probability of the event of going from $\bar{x}$ to the neighborhood of $\bar{y}_0$ is given by setting $\pi(\bar{x}, \bar{y}_0) = |R_s(\bar{x}, \bar{y}_0)|$ and multiplying by the arc element ds, i.e.,

$$|R_s(\bar{x}, \bar{y}_0)|ds = \frac{\cos(\theta_0)ds}{2\pi|\bar{x} - \bar{y}_0|} \tag{C5}$$

if the direction at $\bar{x}$ is isotropically selected from a uniform distribution of angles between $(0, 2\pi)$, and $\bar{y}_0$ is the point where the straight trajectory strikes the boundary, Γ. Similar probabilistic interpretations hold for $|K_s(\bar{y}_{i-1}, \bar{y}_i)|$ and $|R_s(\bar{x}, \bar{y}_0)|$ in 3D in terms of solid angles and surface elements (Nakamura, 1977).

For nonconvex regions, the previous probabilistic interpretation needs to be modified. For example, as shown in Fig. C1, an isotropically chosen straight trajectory emanating from $\bar{x}$ intercepts three boundary points instead of just one boundary point as in the convex case. In this case, $|R_s(\bar{x}, \bar{y}_0)|ds$ should be interpreted as the probability of striking any of the three points along the direction of the straight trajectory; similar modification applies to $|K_s(\bar{y}_{i-1}, \bar{y}_i)|ds$. Note that $\bar{y}_0$ and $\bar{y}_i$ could be any of the three boundary points shown in Fig. C1. More generally, $|R_s(\bar{x}, \bar{y}_0)|ds$ should be interpreted as the probability of striking any of the $q(\bar{y}_0)$ points along the direction of the straight trajectory, where $q(\bar{y}_0)$ is the total number of boundary points intercepted. Similar interpretation applies to $|K_s(\bar{y}_{i-1}, \bar{y}_i)|ds$. Therefore, for nonconvex domains, assuming that each of the $q(\bullet)$ points is equally like to be struck, we have (Sabelfeld, 1991)

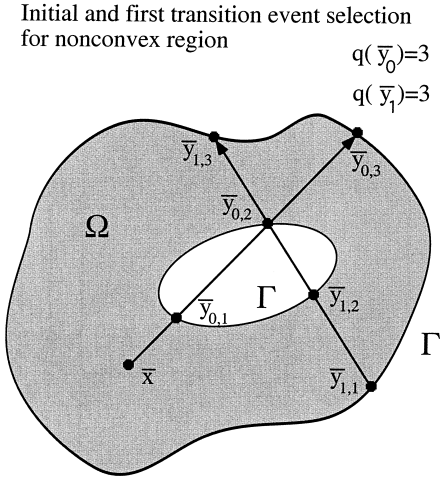

Fig. C1. The schematic illustration of the selection of initial and subsequent boundary points for nonconvex bodies. The initial ray, as illustrated, encountered three boundary points, $\bar{y}_{0,1}$ $\bar{y}_{0,2}$ and $\bar{y}_{0,3}$. Point $\bar{y}_{0,2}$ is selected according to the procedure given in Appendix C. A subsequent ray emanating from $\bar{y}_{0,2}$also encountered three boundary points, $\bar{y}_{1,1}$, $\bar{y}_{1,2}$ and $\bar{y}_{1,3}$. One of these three points can be selected according to the same procedure as given in Appendix C.

$$\pi(\bar{x}, \bar{y}_0) = \frac{|R_s(\bar{x}, \bar{y}_0)|}{q(\bar{y}_0)} \tag{C6a}$$

$$p(\bar{y}_{i-1}, \bar{y}_i) = \frac{|K_s(\bar{y}_{i-1}, \bar{y}_i)|}{q(\bar{y}_i)} \tag{C6b}$$

For two dimensional convex regions, we can generate samples according to the following procedure:

1. For initial events, an isotropic direction is generated by the inverse transform method (Fishman, 1996; Rubinstein, 1981)

$$\theta = 2\pi u \tag{C7}$$

   where θ denotes the direction of the straight trajectory and u is a random number uniformly distributed between (0, 1). The boundary point encountered is then selected.
2. For subsequent events, an isotropic direction is generated by the inverse transform method

$$\theta = \pi u \tag{C8}$$

   The boundary point encountered is then selected.

For three dimensional convex regions, we can generate samples according to the following procedure:

1. For initial events, an isotropic direction is generated by the inverse transform method

$$\theta = 2\pi u \tag{C9a}$$

$$\phi = \arccos(1 - u) \tag{C9b}$$

   where θ is the angle between the projected ray in the x–y plane and the x-axis and ϕ is the angle between the ray and the z-axis. The boundary point encountered is then selected.
2. For subsequent events, an isotropic direction is generated by the inverse transform method

$$\theta = 2\pi u \tag{C10a}$$

$$\phi = \arccos(1 - u/2) \tag{C10b}$$

   The boundary point encountered is then selected.

To generate samples for both two dimensional and three dimensional nonconvex regions, we need only to replace how the boundary points are selected in the convex case by the following procedure:

1. q boundary points are intercepted by the ray generated via the above procedures. These points are indexed as 1, 2,..., q. See Fig. C1 for the case of $q = 3$.
2. Generate a random number, ε, uniformly distributed between (0, 1).
3. Assume the q points are all equally likely to be selected (Sabelfeld, 1991), i.e., if ε falls between $(m-1)/q$ and m/q then the mth point is selected, where m is an integer such that $1 \le m \le q$.

References

Billingsley, P., 1995. Probability and Measure. Wiley, New York.
Brown, G.M., 1956. Modern Mathematics for the Engineer. McGraw-Hill, New York.
Farlow, S.J., 1993. Partial Differential Equations for Scientist and Engineers. Dover, New York.
Fishman, G.S., 1996. Monte Carlo Concept, Algorithms, and Applications. Springer-Verlag, New York.
Grigoriu, M., 1997. Solution of some elasticity problems by the random walk method. Acta Mech 125, 197–209.
Haji-Sheikh, A., Sparrow, E.M., 1966. The floating random walk and its application to Monte Carlo solutions of heat equations. Journal of SIAM, Applied Mathematics 14, 370–389.
Hartman, F., 1989. Introduction to Boundary Elements. Springer-Verlag, New York.
Hilderbrand, F.B., 1965. Methods of Applied Mathematics. Prentice-Hall, Englewood Cliff, NJ.
Hoffman, T.J., Banks, N.E., 1976. Monte Carlo surface density solution to the Dirichlet heat transfer problem. Nuclear Science and Engineering 59, 205–214.
Kanwal, R.P., 1997. Linear Integral Equations Theory and Technique. Birkhauser, Boston.
Mikhailov, G.A., 1992. Optimization of Weighted Monte Carlo Methods. Springer-Verlag, New York.
Minkowycz, W.J., Sparrow, E.M., Schneider, G.E., Pletcher, R.H., 1988. Handbook of Numerical Heat Transfer. Wiley, New York.
Nakamura, S., 1977. Computational Methods in Engineering and Science. Wiley-Interscience, New York.
Parton, V.Z., Perlin, P.I., 1982. Integral Equations in Elasticity. Mir Publishers, Moscow.
Pham, T.L., 1967. Potentiels Elastiques: Tenseurs de Green et de Neumann. J. Mec 6, 211–242.
Ross, S.M., 1997. Simulation. Academic Press, New York.
Rubinstein, R.Y., 1981. Simulation and the Monte Carlo Method. Wiley, New York.
Sabelfeld, K.K., 1991. Monte Carlo Methods in Boundary Value Problems. Springer-Verlag, New York.
Spiegel, M.R., 1995. Schaum's Outline: Statistics. McGraw-Hill, New York.
Zagajac, J., 1996. A fast method for estimating discrete field values in early engineering design. IEEE Transactions on Visualization and Computer Graphics 2, 35–43.